

# Inclusive $\chi_{cJ}$ production in $\Upsilon$ decay at $\mathcal{O}(\alpha_s^5)$ in NRQCD factorization

Zhi-Guo He, Bernd A. Kniehl, Xiang-Peng Wang  
II. Institut für Theoretische Physik, Universität Hamburg,  
Luruper Chaussee 149, 22761 Hamburg, Germany  
(Dated: March 17, 2022)

Inclusive  $\chi_{cJ}$  ( $J = 0, 1, 2$ ) production from  $\Upsilon(1S)$  decay is studied within the framework of nonrelativistic QCD (NRQCD) factorization at leading order in  $v_Q^2$ , which includes the contributions of  $b\bar{b}(^3S_1^{[1]}) \rightarrow c\bar{c}(^3P_J^{[1]}) + X$  and  $b\bar{b}(^3S_1^{[1]}) \rightarrow c\bar{c}(^3S_1^{[8]}) + X$ . For both channels, the short-distance coefficients are calculated through  $\mathcal{O}(\alpha_s^5)$ , which is next-to-leading order for the second one. By fitting to the measured  $\Upsilon(1S)$  branching fractions to  $\chi_{c1}$  and  $\chi_{c2}$ , we obtain the color-octet long-distance matrix element (LDME)  $\langle \mathcal{O}^{\chi_{c0}}(^3S_1^{[8]}) \rangle = (4.04 \pm 0.47_{-0.34}^{+0.67}) \times 10^{-3} \text{ GeV}^3$ , where the first error is experimental and the second one due to the renormalization scale dependence, if we use as input  $\langle \mathcal{O}^{\chi_{c0}}(^3P_0^{[1]}) \rangle = 0.107 \text{ GeV}^5$  as obtained via potential-model analysis. Previous LDME sets, extracted from data of prompt  $\chi_{cJ}$  hadroproduction, yield theoretical predictions that systematically undershoot or mildly overshoot the experimental values of  $\mathcal{B}(\Upsilon \rightarrow \chi_{cJ} + X)$ .

PACS numbers: 12.38.Bx, 12.39.St, 13.25.Gv, 14.40.Pq

## I. INTRODUCTION

Heavy-quarkonium production serves as an ideal laboratory to study both the perturbative and nonperturbative aspects of QCD due to the hierarchy of energy scales  $m_Q v^2 \ll m_Q v \ll m_Q$ , where  $m_Q$  is the mass of the heavy quark  $Q$  and  $v$  is its relative velocity in the rest frame of the heavy meson. The effective quantum field theory of nonrelativistic QCD (NRQCD) [1] endowed with the factorization conjecture of Ref. [2] is the default theoretical approach to study quarkonium production and decay. This conjecture states that the theoretical predictions can be separated into process-dependent short-distance coefficients (SDCs) calculated perturbatively as expansions in the strong-coupling constant  $\alpha_s$  and supposedly universal long-distance matrix elements (LDMEs), scaling with definite power of  $v$  [3]. In this way, the theoretical calculations are organized as double expansion in  $\alpha_s$  and  $v$ .

During the past two decades, the NRQCD factorization approach has celebrated numerous remarkable successes in describing both the production and decay of heavy quarkonium (see Refs. [4, 5] and references therein for a review). However, there are still some challenges in understanding charmonium production, in particular for the  $J/\psi$  meson. Prompt  $J/\psi$  production has been studied in various environments on both experimental and theoretical sides. To date, the SDCs are available at next-to-leading order (NLO) in  $\alpha_s$  for the yield [6, 7] and polarization [8] in  $e^+e^-$  annihilation, the yield in two-photon collisions [9, 10], the yield [11] and polarization [12] in photoproduction, the yield [13, 14] and polarization [15–18] in hadroproduction, etc. Different sets of LDMEs were obtained by fitting experimental data adopting different strategies. Unfortunately, none of them can explain all the experimental measurements,

which challenges the universality of the NRQCD LDMEs. Recently, it has been found that all the LDME sets determined from  $J/\psi$  production data result in NLO predictions that overshoot the  $\eta_c$  hadroproduction data [19].

Because the P-wave states  $\chi_{cJ}$  ( $J = 1, 2$ ) have substantial branching fractions to  $J/\psi$  though  $\chi_{cJ} \rightarrow J/\psi + \gamma$ , their production can also be measured, which provides an additional playground to test the NRQCD factorization hypothesis. Moreover, the feed-down contributions from the  $\chi_{c1}$  and  $\chi_{c2}$  mesons to the yield and polarization of prompt  $J/\psi$  hadroproduction is sizable [17, 20]. Unlike for the  $J/\psi$  meson, inclusive  $\chi_{cJ}$  production has only been studied in a few processes, for example hadroproduction [17, 20–23],  $e^+e^-$  annihilation [24], top-quark decay [25],  $B$  hadron decay [26], and  $\eta_b$  meson decay [27, 28].

In this work, we will study another interesting process, namely inclusive  $\chi_{cJ}$  production through  $\Upsilon(1S)$  decay. On the experimental side, thanks to the large number of  $\Upsilon(1S)$  decay events collected with the Belle detector,  $102 \times 10^6$ , the value  $\mathcal{B}(\Upsilon(1S) \rightarrow \chi_{c1} + X) = (1.90 \pm 0.35) \times 10^{-4}$  has recently been obtained [29], which is more precise than the previous result  $(2.3 \pm 0.7) \times 10^{-4}$  extracted by analyzing  $21.2 \times 10^6$   $\Upsilon(1S)$  decay events collected with the CLEO III detector [30]. As for  $\mathcal{B}(\Upsilon(1S) \rightarrow \chi_{c2} + X)$ , the combined result  $(2.8 \pm 0.8) \times 10^{-4}$  was reported by the Particle Data Group in 2016 [31].

This process was considered theoretically more than two decades ago in Refs. [32, 33], where the contributions of  $c\bar{c}$  pairs in color singlet (CS) ( $^3P_J^{[1]}$ ) and color octet (CO) ( $^3S_1^{[8]}$ ) Fock states were computed at leading order (LO) in  $\alpha_s$ . Moreover, in Ref. [32], a cut on the soft-gluon energy was introduced to regularize the infrared (IR) divergences.

Many of the theoretical works mentioned above have shown that the effects of NLO QCD corrections may be large. Therefore, in this work, we calculate the NLO

QCD corrections to inclusive  $\chi_{cJ}$  production by  $\Upsilon$  decay within the framework of NRQCD factorization. Note that we do not take into account the contributions from  $b\bar{b}$  pairs in CO states, since they are suppressed by  $v_b^4$ . The remainder of this paper is organized as follows. In Sec. II, we describe how to calculate the relevant SDCs in detail. In Sec. III, we present the numerical results and compare them with the available experimental measurements. In Sec. IV, we summarize our results. In Appendix A, we list the master integrals arising in the virtual corrections through  $\mathcal{O}(\epsilon)$  in the expansion parameter of dimensional regularization. In Appendix B, we list the soft integrals arising in the real corrections implemented with phase space slicing.

## II. CALCULATION OF SDCS

### A. NRQCD Factorization and Notations

In the NRQCD factorization formalism, at LO in  $v_b$  and  $v_c$ , the decay width of  $\Upsilon \rightarrow \chi_{cJ} + X$  can be written as

$$\begin{aligned} \Gamma(\Upsilon \rightarrow \chi_{cJ} + X) &= \langle \Upsilon | \mathcal{O}(^3S_1^{[1]}) | \Upsilon \rangle \\ &\times \left[ \hat{\Gamma}_1 \left( b\bar{b}(^3S_1^{[1]}) \rightarrow c\bar{c}(^3P_J^{[1]}) + X \right) \langle \mathcal{O}^{\chi_{cJ}}(^3P_J^{[1]}) \rangle \right. \\ &\left. + \hat{\Gamma}_8 \left( b\bar{b}(^3S_1^{[1]}) \rightarrow c\bar{c}(^3S_1^{[8]}) + X \right) \langle \mathcal{O}^{\chi_{cJ}}(^3S_1^{[8]}) \rangle \right], \quad (1) \end{aligned}$$

where  $\hat{\Gamma}_1$  and  $\hat{\Gamma}_8$  are the SDCs and  $\langle \Upsilon | \mathcal{O}(^3S_1^{[1]}) | \Upsilon \rangle$ ,  $\langle \mathcal{O}^{\chi_{cJ}}(^3P_J^{[1]}) \rangle$ , and  $\langle \mathcal{O}^{\chi_{cJ}}(^3S_1^{[8]}) \rangle$  are the LDMEs. We adopt the conventions for the LDMEs introduced in Ref. [2]. The LDMEs for  $\chi_{cJ}$  production satisfy the multiplicity relations

$$\begin{aligned} \langle \mathcal{O}^{\chi_{cJ}}(^3P_J^{[1]}) \rangle &= (2J+1) \langle \mathcal{O}^{\chi_{c0}}(^3P_0^{[1]}) \rangle, \\ \langle \mathcal{O}^{\chi_{cJ}}(^3S_1^{[8]}) \rangle &= (2J+1) \langle \mathcal{O}^{\chi_{c0}}(^3S_1^{[8]}) \rangle, \quad (2) \end{aligned}$$

which follow from heavy-quark spin symmetry at LO in  $v_c$ .

At LO in  $\alpha_s$ , at  $\mathcal{O}(\alpha_s^4)$ , only the CO subprocess  $b\bar{b}(^3S_1^{[1]}) \rightarrow c\bar{c}(^3S_1^{[8]}) + gg$  contributes, and its NLO QCD corrections include both virtual and real corrections at  $\mathcal{O}(\alpha_s^5)$ . CS contributions start to contribute at  $\mathcal{O}(\alpha_s^5)$  via  $b\bar{b}(^3S_1^{[1]}) \rightarrow c\bar{c}(^3P_J^{[1]}) + ggg$ . We will calculate this consistently in dimensional regularization, with  $D = 4 - 2\epsilon$  space-time dimensions.

Moreover, inclusive  $J/\psi$  production by  $e^+e^-$  annihilation [34–37] and  $\Upsilon$  decay [38] is known to receive substantial contributions from events that also contain an open  $c\bar{c}$  pair in the final state. This motivates us to include the contributions from  $b\bar{b}(^3S_1^{[1]}) \rightarrow c\bar{c}(^3P_J^{[1]}) + c\bar{c}g$  and  $b\bar{b}(^3S_1^{[1]}) \rightarrow c\bar{c}(^3S_1^{[8]}) + c\bar{c}g$  at  $\mathcal{O}(\alpha_s^5)$  as well. A similar study of  $J/\psi$  production by  $\Upsilon$  decay in the NRQCD factorization approach will be presented in a forthcoming paper [39] and compared with previous investigations [32, 33, 38, 40, 41].

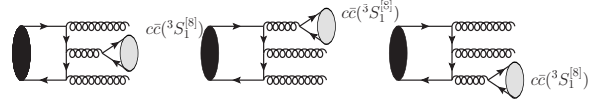


FIG. 1: Typical tree-level Feynman diagrams for the partonic subprocess  $b\bar{b}(^3S_1^{[1]}) \rightarrow c\bar{c}(^3S_1^{[8]}) + gg$ .

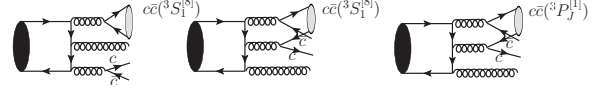


FIG. 2: Typical tree-level Feynman diagrams for the partonic subprocess  $b\bar{b}(^3S_1^{[1]}) \rightarrow c\bar{c}(^3S_1^{[8]}/^3P_J^{[1]}) + c\bar{c}g$ .

There are 6 Feynman diagrams for the partonic subprocess  $b\bar{b}(^3S_1^{[1]}) \rightarrow c\bar{c}(^3S_1^{[8]}) + gg$  at tree level (see Fig. 1). The analytical and numerical results were first presented in Ref. [33], and we reproduce them. To compute the NLO QCD corrections, the analytical expression for the scattering amplitude must also be obtained in  $D$  dimensions. Ultraviolet (UV) and IR divergences are encountered in the calculation of the NLO QCD corrections to  $b\bar{b}(^3S_1^{[1]}) \rightarrow c\bar{c}(^3S_1^{[8]}) + gg$ . IR divergences also appear in the phase space integration of the subprocesses  $b\bar{b}(^3S_1^{[1]}) \rightarrow c\bar{c}(^3P_J^{[1]}) + ggg$ . We will present in detail the treatment of these divergences in dimensional regularization in the next three subsections. The calculation of the associated open-charm subprocesses (Fig. 2) is straightforward because no divergences appear in the phase space integrations. Their analytical expressions are too lengthy to be displayed here, and we thus only present the numerical results for them in the next section.

In our analytical computation, the Feynman diagrams are generated using FeynArts [42]. Algebraic operations such as color and Dirac algebra are performed with FeynCalc [43] and FORM [44]. For the virtual corrections, we use the Mathematica package \$Apart [45] to decompose linearly dependent propagators in the loop integrals to irreducible ones. The latter are then reduced to master scalar integrals using the FIRE [46] package. The master integrals are evaluated numerically using the C++ package QCDLOOP [47]. Finally, the phase space integrations are performed numerically with the help of the CUBA [48] library.

### B. Virtual Corrections

Typical Feynman diagrams of the virtual corrections are shown in Fig. 3. They fall into four groups, including self-energy diagrams, vertex correction diagrams, counterterm diagrams, and diagrams that are generated from tree-level diagrams of Fig. 1 by attaching one virtual-gluon line in all other possible ways.

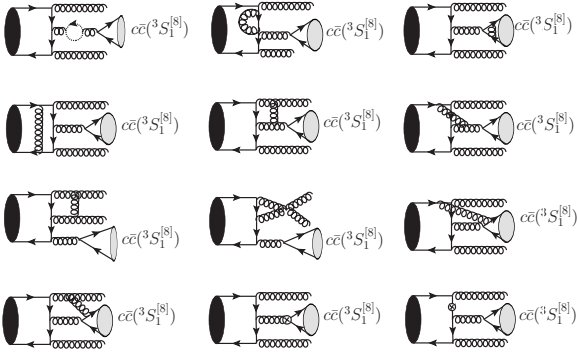


FIG. 3: Typical Feynman diagrams for the virtual corrections to the partonic subprocess  $b\bar{b}({}^3S_1^{[1]}) \rightarrow c\bar{c}({}^3S_1^{[8]}) + gg$ .

In the analytical calculation of the tree-level subprocess  $b\bar{b}({}^3S_1^{[1]})(P) \rightarrow c\bar{c}({}^3S_1^{[8]})(K) + g(k_3)g(k_4)$  and the corresponding virtual corrections, the Mandelstam variables are defined as

$$s \equiv (P - k_4)^2, \quad t \equiv (P - K)^2, \quad u \equiv (P - k_3)^2, \quad (3)$$

so that  $s + u + t = 4m_b^2 + 4m_c^2$ , where  $m_c$  and  $m_b$  are the masses of the charm and bottom quarks, respectively. For convenience, we also introduce

$$\begin{aligned} s_c &\equiv s - 4m_c^2, & s_b &\equiv 4m_b^2 - s, \\ u_c &\equiv u - 4m_c^2, & u_b &\equiv 4m_b^2 - s. \end{aligned} \quad (4)$$

Labeling the tree-level amplitude and the amplitude of the virtual corrections as  $\mathcal{M}_{\text{Born}}$  and  $\mathcal{M}_{\text{virtual}}$ , respectively, the SDC of the virtual corrections is evaluated as

$$d\hat{\Gamma}^{\text{VC}} = \frac{1}{4m_b} d\text{PS}_{1 \rightarrow 3} \sum 2\text{Re}(\mathcal{M}_{\text{Born}}^* \mathcal{M}_{\text{virtual}}), \quad (5)$$

where  $d\text{PS}_{1 \rightarrow 3}$  is the three-body phase space and  $\sum$  implies average over the color and polarization states.

The UV divergences are removed through renormalization. We adopt a mixed renormalization scheme [9], in which the renormalization constants  $Z_2$ ,  $Z_m$ , and  $Z_3$  of the heavy-quark field  $\psi_Q$ , heavy-quark mass  $m_Q$ , and gluon field  $A_\mu^a$  are defined in the on-shell (OS) scheme, while the renormalization constant  $Z_g$  of the strong-coupling  $g_s$  is defined in modified minimal-subtraction ( $\overline{\text{MS}}$ ) scheme. At the one-loop level, they read

$$\delta Z_g^{\overline{\text{MS}}} = -\frac{\beta_0}{2} \frac{\alpha_s}{4\pi} C_\epsilon \frac{1}{\epsilon_{\text{UV}}}, \quad (6)$$

$$\delta Z_2^{\text{OS}} = -C_F \frac{\alpha_s}{4\pi} C_\epsilon \left[ \frac{1}{\epsilon_{\text{UV}}} + \frac{2}{\epsilon_{\text{IR}}} + 3 \ln \frac{\mu^2}{m^2} + 4 \right], \quad (7)$$

$$\delta Z_3^{\text{OS}} = \frac{\alpha_s}{4\pi} C_\epsilon (\beta_0 - 2C_A) \left[ \frac{1}{\epsilon_{\text{UV}}} - \frac{1}{\epsilon_{\text{IR}}} \right], \quad (8)$$

$$\delta Z_m^{\text{OS}} = -3C_F \frac{\alpha_s}{4\pi} C_\epsilon \left[ \frac{1}{\epsilon_{\text{UV}}} + \ln \frac{\mu^2}{m^2} + \frac{4}{3} \right], \quad (9)$$

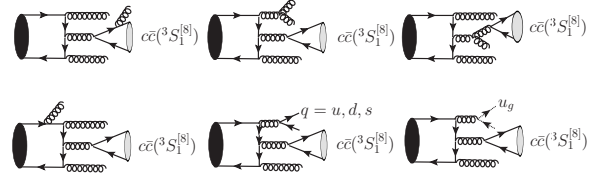


FIG. 4: Typical Feynman diagrams for the real corrections to the partonic subprocess  $b\bar{b}({}^3S_1^{[1]}) \rightarrow c\bar{c}({}^3S_1^{[8]}) + gg$ .

where  $C_\epsilon = (4\pi e^{-\gamma_E})^\epsilon$ ,  $\mu$  is the renormalization scale, and  $\beta_0 = (11/3)C_A - (4/3)T_F n_f$  is the one-loop coefficient of the QCD beta function. We have  $n_f = 3$  active quark flavors in our calculation. In Eqs. (7) and (9),  $m$  is to be substituted by  $m_c$  and  $m_b$  for charm and bottom, respectively.

At the end of the reduction done with FIRE [46], the loop corrections are expressed in terms of some master integrals. Among them, the coefficients of some tadpole and bubble integrals carry extra poles  $\frac{1}{\epsilon}$ . Therefore, we must calculate these integrals through  $\mathcal{O}(\epsilon)$ . The results are given in Appendix A. We extract the divergences analytically and find that they cancel after combination with the real corrections, which are IR divergent.

### C. Real Corrections

In our calculation of the real corrections, we choose Feynman gauge with the polarization sum of the gluon given by

$$\sum_{\text{pol}^*} \epsilon_\mu \epsilon_\nu^* = -g_{\mu\nu}. \quad (10)$$

Consequently, the nonphysical degrees of freedom due to the gluon-ghost contributions should be subtracted as

$$\begin{aligned} &\sum_{\text{col, pol}} |\mathcal{M}(b\bar{b}({}^3S_1^{[1]}) \rightarrow c\bar{c}({}^3S_1^{[8]}) + ggg)|^2 \\ &= \sum_{\text{col, pol}^*} \left( |\mathcal{M}(b\bar{b}({}^3S_1^{[1]}) \rightarrow c\bar{c}({}^3S_1^{[8]}) + ggg)|^2 \right. \\ &\quad - 2|\mathcal{M}(b\bar{b}({}^3S_1^{[1]}) \rightarrow c\bar{c}({}^3S_1^{[8]}) + g u_g(k_4) \bar{u}_g(k_5))|^2 \\ &\quad - 2|\mathcal{M}(b\bar{b}({}^3S_1^{[1]}) \rightarrow c\bar{c}({}^3S_1^{[8]}) + u_g(k_3) g \bar{u}_g(k_5))|^2 \\ &\quad \left. - 2|\mathcal{M}(b\bar{b}({}^3S_1^{[1]}) \rightarrow c\bar{c}({}^3S_1^{[8]}) + u_g(k_3) \bar{u}_g(k_4) g)|^2 \right), \end{aligned} \quad (11)$$

where  $u_g$  and  $\bar{u}_g$  stand for the ghost and antighost, respectively.

In this way, we have to calculate (see Fig. 4)  $b\bar{b}({}^3S_1^{[1]})(P) \rightarrow c\bar{c}({}^3S_1^{[8]})(K) + g(k_3)g(k_4)g(k_5)$  (96 Feynman diagrams) and  $b\bar{b}({}^3S_1^{[1]}) \rightarrow c\bar{c}({}^3S_1^{[8]}) + g u_g \bar{u}_g / u_g g \bar{u}_g / u_g \bar{u}_g g / q \bar{q} g$  (6 Feynman diagrams for each

subprocess). These subprocesses share the same kinematics, for which we define

$$\begin{aligned} s_1 &\equiv (P - K)^2, \quad s_2 \equiv (P - K - k_4)^2, \quad u_1 \equiv (P - k_4)^2, \\ u_2 &\equiv (P - k_5)^2, \quad t_2 \equiv (P - k_4 - k_5)^2. \end{aligned} \quad (12)$$

In the phase space integrations of the above subprocesses, we encounter soft, collinear, and soft-collinear divergences, which we subtract by means of the phase space slicing method [49]. Specifically, we introduce two slicing parameters,  $\delta_s$  and  $\delta_c$ , to demarcate the soft regions as

$$\frac{E_3}{m_c} < \delta_s \text{ or } \frac{E_4}{m_c} < \delta_s \text{ or } \frac{E_5}{m_c} < \delta_s, \quad (13)$$

and the collinear regions as

$$s_{34} < \delta_c m_c^2 \text{ or } s_{35} < \delta_c m_c^2 \text{ or } s_{45} < \delta_c m_c^2, \quad (14)$$

where  $E_3$ ,  $E_4$ , and  $E_5$  are the energies of the soft gluons with momenta  $k_3$ ,  $k_4$ , and  $k_5$ , respectively, and  $s_{34} = (k_3 + k_4)^2$ ,  $s_{35} = (k_3 + k_5)^2$ ,  $s_{45} = (k_4 + k_5)^2$ . In our case, where three identical gluons are in the final state, it is sufficient to subtract the soft and collinear divergences in one of the soft regions in Eq. (13) and one of the collinear regions in Eq. (14).

### 1. Soft Region

As an example, let us consider the case when  $k_5$  is soft, which implies that  $E_5 < \delta_s m_c$ . We parametrize the momenta in the center-of-mass frame of  $P$  and  $-K$ , which, at the same time, is the center-of-mass frame of  $k_3$  and  $k_4$  in the limit  $k_5 \rightarrow 0$ , as

$$\begin{aligned} P &= (E_P, 0, |\mathbf{p}| \sin \theta, |\mathbf{p}| \cos \theta), \\ K &= (E_K, 0, |\mathbf{p}| \sin \theta, |\mathbf{p}| \cos \theta), \\ k_3 &= E_3(1, 0, 0, 1), \\ k_4 &= E_4(1, 0, 0, -1), \\ k_5 &= E_5(1, \sin \theta_1 \sin \theta_2, \sin \theta_1 \cos \theta_2, \cos \theta_1), \end{aligned} \quad (15)$$

where

$$\begin{aligned} E_P &= \frac{s_b + u_b}{2\sqrt{t}}, \quad E_K = \frac{s_c + u_c}{2\sqrt{t}}, \quad E_3 = E_4 = \frac{\sqrt{t}}{2}, \\ |\mathbf{p}| &= \frac{a}{2\sqrt{t}}, \quad \cos \theta = \frac{u - s}{a}, \end{aligned} \quad (16)$$

with  $a = \sqrt{(s + u)^2 - 64m_c^2 m_b^2}$ .

The corresponding contribution from the soft region to the real corrections is given by

$$d\hat{\Gamma}_{k_5 \text{ soft}}^{\text{RC}} = \frac{1}{4m_b} d\text{PS}_{1 \rightarrow 3} \int_{\text{soft}} d\text{PS}_{k_5} \sum \overline{|\mathcal{M}_{k_5 \text{ soft}}|^2}, \quad (17)$$

where

$$\begin{aligned} \int_{\text{soft}} d\text{PS}_{k_5} &\equiv \int_{\text{soft}} \frac{\mu^{4-D} d^{D-1} k_5}{2(2\pi)^{D-1} E_5} = \frac{(\pi \mu^2)^\epsilon \Gamma(1 - \epsilon)}{(2\pi)^3 \Gamma(1 - 2\epsilon)} \\ &\times \int_0^{\delta_s m_c} E_5^{1-2\epsilon} dE_5 \int_0^\pi \sin \theta_1^{1-2\epsilon} d\theta_1 \int_0^\pi \sin \theta_2^{-2\epsilon} d\theta_2. \end{aligned} \quad (18)$$

Therefore, in the limit  $k_5 \rightarrow 0$ , we have

$$\begin{aligned} d\hat{\Gamma}_{k_5 \text{ soft}}^{\text{RC}} &= d\hat{\Gamma}^{\text{LO}}(b\bar{b}(^3S_1^{[1]}) \rightarrow c\bar{c}(^3S_1^{[8]}) + gg) \\ &\times \frac{3}{2} \int_{\text{soft}} d\text{PS}_{k_5} \left[ \frac{t}{(k_3 \cdot k_5)(k_4 \cdot k_5)} - \frac{8m_c^2}{(K \cdot k_5)^2} \right. \\ &\quad \left. + \frac{u_c}{(k_4 \cdot k_5)(K \cdot k_5)} + \frac{s_c}{(k_3 \cdot k_5)(K \cdot k_5)} \right], \end{aligned} \quad (19)$$

where  $\hat{\Gamma}^{\text{LO}}(b\bar{b}(^3S_1^{[1]}) \rightarrow c\bar{c}(^3S_1^{[8]}) + gg)$  is calculated in  $D$  dimensions and the results of the soft integrals are listed in Appendix B.

### 2. Hard-Collinear Region

Let us assume that  $k_4$  is collinear to  $k_5$ . Then the SDC can be factorized as

$$\begin{aligned} d\hat{\Gamma}_{4' \rightarrow 45, \text{hard}} &= d\hat{\Gamma}^{\text{LO}}(b\bar{b}(^3S_1^{[1]}) \rightarrow c\bar{c}(^3S_1^{[8]}) + ggg) \\ &= d\hat{\Gamma}^{\text{LO}}(b\bar{b}(^3S_1^{[1]}) \rightarrow c\bar{c}(^3S_1^{[8]}) + gg) \frac{3g_s^2}{8\pi^2} \left( \frac{4\pi\mu^2 e^{-\gamma_E}}{m_c^2} \right)^\epsilon \\ &\times \left[ \left( 2 \ln \frac{2\delta_s m_c}{\sqrt{t}} + \frac{11}{6} \right) \left( \frac{1}{\epsilon} - \ln \delta_c \right) - \ln^2 \frac{2\delta_s m_c}{\sqrt{t}} \right. \\ &\quad \left. + \frac{67}{18} - \frac{\pi^2}{3} \right] \end{aligned} \quad (20)$$

for  $g \rightarrow gg$  splitting and

$$\begin{aligned} d\hat{\Gamma}_{4' \rightarrow 45, \text{hard}} &= d\hat{\Gamma}^{\text{LO}}(b\bar{b}(^3S_1^{[1]}) \rightarrow c\bar{c}(^3S_1^{[8]}) + g + q\bar{q}) \\ &= d\hat{\Gamma}^{\text{LO}}(b\bar{b}(^3S_1^{[1]}) \rightarrow c\bar{c}(^3S_1^{[8]}) + gg) \\ &\times \frac{g_s^2}{24\pi^2} \left( \frac{4\pi\mu^2 e^{-\gamma_E}}{m_c^2} \right)^\epsilon \left( -\frac{1}{\epsilon} + \ln \delta_c - \frac{5}{3} \right) \end{aligned} \quad (21)$$

for  $g \rightarrow q\bar{q}$  splitting.

In the case of  $g \rightarrow gg$  splitting, hard conditions for the splitting gluons are applied to avoid double counting of the soft-collinear region.

### 3. Hard-Noncollinear Region

In the hard-noncollinear region, the phase space integration is finite, so that we can directly perform the numerical integration in four dimensions. In the rest frame of  $P$  and  $-K$ , the conditions defining the hard-noncollinear region are given by

$$\begin{aligned} E_3 &= \frac{s_1 + u_1 + u_2 - t_2 - 4m_b^2}{2\sqrt{s_1}} > \delta_s m_c, \\ E_4 &= \frac{s_1 - s_2}{2\sqrt{s_1}} > \delta_s m_c, \\ E_5 &= \frac{t_2 + s_2 - u_1 - u_2 + 4m_b^2}{2\sqrt{s_1}} > \delta_s m_c, \\ s_{34} &= s_1 + u_1 + u_2 - t_2 - s_2 - 4m_b^2 > \delta_c m_c^2, \\ s_{35} &= s_2 > \delta_c m_c^2, \\ s_{45} &= 4m_b^2 + t_2 - u_1 - u_2 > \delta_c m_c^2. \end{aligned} \quad (22)$$

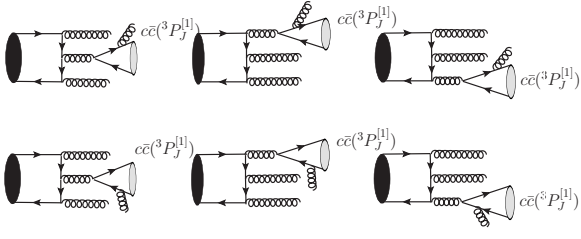


FIG. 5: Typical tree-level Feynman diagrams for the partonic subprocess  $b\bar{b}(^3S_1^{[1]}) \rightarrow c\bar{c}(^3P_J^{[1]}) + ggg$ .

We express the four-body phase space in covariant form [50], so that these conditions can be easily implemented in the numerical phase space integration. Combining the contributions from the soft, hard-collinear, and hard-noncollinear regions, the numerical results converge as  $\delta_s$  becomes small ( $\delta_s < 10^{-2}$ ) with  $\delta_c$  being much smaller than  $\delta_s$ . Specifically, we choose  $\delta_c = \delta_s/100$ .

#### D. $b\bar{b}(^3S_1^{[1]}) \rightarrow c\bar{c}(^3P_J^{[1]}) + ggg$

There are 36 Feynman diagrams for the tree-level subprocess  $b\bar{b}(^3S_1^{[1]}) \rightarrow c\bar{c}(^3P_J^{[1]}) + ggg$  (see Fig. 5). As expected, IR divergences appear in the phase space integration. In NRQCD factorization, this kind of IR divergences are absorbed into the NLO corrections to the respective CO LDME  $\langle \mathcal{O}^{\chi_{cJ}}(^3S_1^{[8]}) \rangle$  [2, 51],

$$\begin{aligned} \langle \mathcal{O}^{\chi_{cJ}}(^3S_1^{[8]}) \rangle_{\text{Born}} &= \langle \mathcal{O}^{\chi_{cJ}}(^3S_1^{[8]}) \rangle_{\text{ren}} \\ &+ \frac{2\alpha_s}{3\pi m_c^2} \left( \frac{4\pi\mu^2}{\mu_\Lambda^2} e^{-\gamma_E} \right)^\epsilon \frac{1}{\epsilon_{\text{IR}}} \sum_J \left[ \frac{C_F}{C_A} \langle \mathcal{O}^{\chi_{cJ}}(^3P_J^{[1]}) \rangle_{\text{Born}} \right. \\ &\left. + \left( \frac{C_A}{2} - \frac{2}{C_A} \right) \langle \mathcal{O}^{\chi_{cJ}}(^3P_J^{[8]}) \rangle_{\text{Born}} \right], \end{aligned} \quad (23)$$

where  $\langle \mathcal{O}^{\chi_{cJ}}(^3S_1^{[8]}) \rangle_{\text{ren}}$  is the renormalized LDME and  $\mu_\Lambda$  is the renormalization scale of the LDME  $\langle \mathcal{O}^{\chi_{cJ}}(^3S_1^{[8]}) \rangle$ .

Here, we adopt the same approach as in the computation of the real corrections to  $b\bar{b}(^3S_1^{[1]}) \rightarrow c\bar{c}(^3S_1^{[8]}) + ggg$  to extract the IR divergences, except that only one slicing parameter, namely  $\delta_s$ , is needed. Let us consider the limit of  $k_5$  being soft as an example, in which the squared matrix element can be factorized as

$$\begin{aligned} |\mathcal{M}(b\bar{b}(^3S_1^{[1]}) \rightarrow c\bar{c}(^3P_J^{[1]}) + ggg)|_{k_5\text{soft}}^2 \\ = 4g_s^2 \frac{\epsilon^{\beta'}(k_5) \epsilon^{*\beta}(k_5) \epsilon_{\alpha\beta}^{(J)*}(K) \epsilon_{\alpha'\beta'}^{(J)}(K)}{(K \cdot k_5)^2} \\ \times \mathcal{M}_{\text{Born}}^\alpha(T_c - T_{\bar{c}})(T_c - T_{\bar{c}}) \mathcal{M}_{\text{Born}}^{*\alpha'}, \end{aligned} \quad (24)$$

where  $\epsilon^{\beta'}(k_5)$  and  $\epsilon_{\alpha\beta}^{(J)*}(K)$  are the polarization vector and tensor of the soft gluon and  $c\bar{c}$  pair,  $T_c$  and  $T_{\bar{c}}$  are the color matrices corresponding to the soft-gluon

attachments to the charm and anticharm quark lines, and  $\mathcal{M}_{\text{Born}}^\alpha$  is the amplitude of the Born-level subprocess  $b\bar{b}(^3S_1^{[1]}) \rightarrow c\bar{c}(^3S_1^{[8]}) + gg$ , with  $\alpha$  being the Lorentz index of the polarization vector of the  $c\bar{c}$  pair.

Choosing axial gauge for the soft gluon, with polarization sum

$$\begin{aligned} \sum_{\text{pol}} \epsilon_{\beta'}(k_5) \epsilon_\beta^*(k_5) \\ = -g_{\beta'\beta} + \frac{K_{\beta'} k_{5\beta} + K_\beta k_{5\beta'}}{K \cdot k_5} - \frac{K^2 k_{5\beta'} k_{5\beta}}{(K \cdot k_5)^2}, \end{aligned} \quad (25)$$

the contribution from the region where  $k_5$  is soft then reads

$$\begin{aligned} d\hat{\Gamma}_{k_5\text{soft}} &= \frac{1}{4m_b} d\text{PS}_{1 \rightarrow 3} \int_{\text{soft}} d\text{PS}_{k_5} \\ &\times \overline{\sum} |\mathcal{M}(b\bar{b}(^3S_1^{[1]}) \rightarrow c\bar{c}(^3P_J^{[1]}) + ggg)|_{k_5\text{soft}}^2 \\ &= \frac{1}{4m_b} d\text{PS}_{1 \rightarrow 3} \int_{\text{soft}} d\text{PS}_{k_5} \frac{4g_s^2}{(K \cdot k_5)^2} \\ &\times \left( -g_{\beta'\beta} + \frac{K_{\beta'} k_{5\beta} + K_\beta k_{5\beta'}}{K \cdot k_5} - \frac{K^2 k_{5\beta'} k_{5\beta}}{(K \cdot k_5)^2} \right) \\ &\times \overline{\sum} \epsilon_{\alpha\beta}^{(J)*} \epsilon_{\alpha'\beta'}^{(J)} \mathcal{M}_{\text{Born}}^\alpha(T_c - T_{\bar{c}})(T_c - T_{\bar{c}}) \\ &\times \mathcal{M}_{\text{Born}}^{*\alpha'}. \end{aligned} \quad (26)$$

Now we tackle the new type of tensor integral  $\int_{\text{soft}} d\text{PS}_{k_5} \frac{k_{5\beta} k_{5\beta'}}{(K \cdot k_5)^4}$ . This cannot be reduced to scalar integrals through conventional tensor reduction procedures, since it is not Lorentz covariant due to the cut-off in the soft-gluon energy. Therefore, we explicitly evaluate these tensor integrals as they appear, e.g. as  $\int_{\text{soft}} d\text{PS}_{k_5} \frac{(k_3 \cdot k_5)(k_4 \cdot k_5)}{(K \cdot k_5)^4}$ . As a result, the  $D$ -dimensional Born-level squared matrix element of subprocess  $b\bar{b}(^3S_1^{[1]}) \rightarrow c\bar{c}(^3S_1^{[8]}) + gg$  does not factorize from the  $D$ -dimensional squared matrix elements of subprocess  $b\bar{b}(^3S_1^{[1]}) \rightarrow c\bar{c}(^3P_J^{[1]}) + ggg$  in the soft limit. This is different from the case of the real corrections. Nevertheless, this does not affect the cancellation of IR divergences, since the divergences appear to be proportional to the four-dimensional Born-level squared matrix element of subprocess  $b\bar{b}(^3S_1^{[1]}) \rightarrow c\bar{c}(^3S_1^{[8]}) + gg$ .

### III. PHENOMENOLOGICAL RESULTS

We are now in the position to present our numerical analysis of inclusive  $\chi_{cJ}$  production in  $\Upsilon$  decay at  $\mathcal{O}(\alpha_s^5)$  in the NRQCD factorization framework. We first list our input parameters. We take the quark pole masses to be  $m_c = m_{J/\psi}/2 = 1.5$  GeV and  $m_b = m_\Upsilon/2 = 4.75$  GeV, and fix the NRQCD factorization scale to be  $\mu_\Lambda = m_c$ . For consistency, we employ the one-loop (two-loop) formula for  $\alpha_s(\mu)$  [31] in the LO (NLO) part of our analysis, with  $n_f = 3$  active quark flavors and asymptotic scale parameter  $\Lambda_{\text{QCD}} = 249$  MeV (389 MeV).

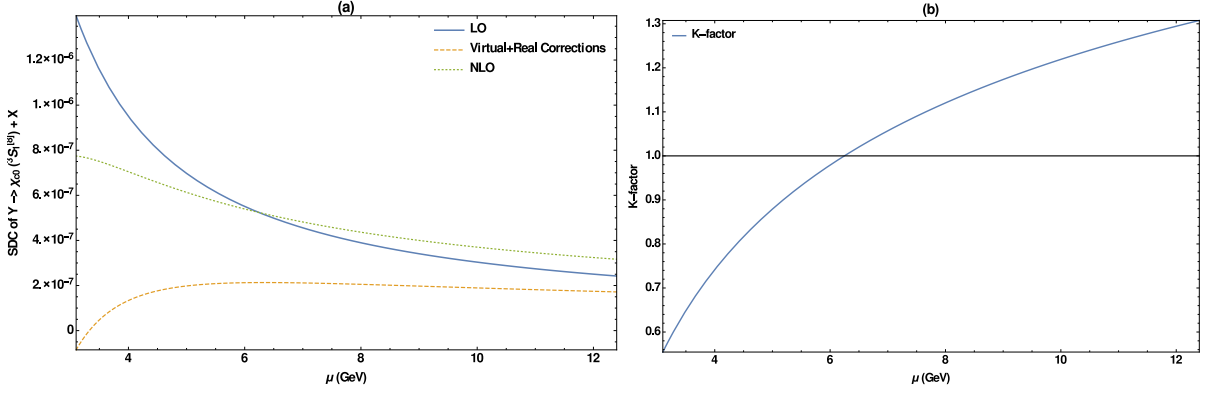


FIG. 6:  $\mu$  dependencies of (a)  $\hat{\Gamma}_{8,gg}^{\text{LO}}$ ,  $\hat{\Gamma}_{8,gg}^{\text{corr}}$ , and  $\hat{\Gamma}_{8,gg}^{\text{NLO}}$  and (b)  $K$  factor.

Adopting the value  $|R'_{1P}(0)| = 0.075 \text{ GeV}^5$  of the first derivative of the wave function at the origin obtained in Ref. [52] for the Buchmüller-Tye potential [53], we have  $\langle \mathcal{O}^{\chi_{c0}} ({}^3P_0^{[1]}) \rangle = 0.107 \text{ GeV}^5$ . As for the CO LDME  $\langle \mathcal{O}^{\chi_{c0}} ({}^3S_1^{[8]}) \rangle$ , we use the results  $(2.21 \pm 0.12) \times 10^{-3} \text{ GeV}^3$  [17] and  $(2.2_{-0.3}^{+0.5}) \times 10^{-3} \text{ GeV}^3$  [20] extracted by fitting to experimental data of  $\chi_{cJ}$  hadroproduction.

We start by investigating the sizes and  $\mu$  dependencies of the SDCs of the individual partonic subprocesses. It is convenient to write:

$$\begin{aligned} \hat{\Gamma}_{8,gg}^{\text{LO}} &= f_{8,gg}^{\text{LO}}(m_c, m_b) \alpha_s^4(\mu) \text{ GeV}^{-5}, \\ \hat{\Gamma}_{8,gg}^{\text{corr}} &= f_{8,gg}^{\text{corr}}(m_c, m_b, \mu) \alpha_s^5(\mu) \text{ GeV}^{-5}, \\ \hat{\Gamma}_{8,c\bar{c}g} &= f_{8,c\bar{c}g}(m_c, m_b) \alpha_s^5(\mu) \text{ GeV}^{-5}, \\ \hat{\Gamma}_{1,ggg}^J &= f_{1,ggg}^J(m_c, m_b) \alpha_s^5(\mu) \text{ GeV}^{-7}, \\ \hat{\Gamma}_{1,c\bar{c}g}^J &= f_{1,c\bar{c}g}^J(m_c, m_b) \alpha_s^5(\mu) \text{ GeV}^{-7}, \end{aligned} \quad (27)$$

where  $\hat{\Gamma}_{1/8,X}^J$  is the SDC of partonic subprocess  $\Upsilon ({}^3S_1^{[1]}) \rightarrow \chi_{cJ} ({}^3P_J^{[1]}/{}^3S_1^{[8]}) + X$ , and the alternative labels "LO" and "corr" stand for the LO contribution and the radiative correction to it. Our numerical results for the dimensionless factors  $f_{1/8,X}$  are listed in Table I. From there, we observe that there are strong numerical cancellations between the  $c\bar{c} ({}^3P_J^{[1]})$  and  $c\bar{c} ({}^3S_1^{[8]})$  channels. In fact, the entries for  $f_{1,ggg}^J$  in Table I are negative and do not carry any physical meaning by themselves. This may be understood by observing that the CS SDCs of  $b\bar{b} ({}^3S_1^{[1]}) \rightarrow c\bar{c} ({}^3P_J^{[1]}) + ggg$  are IR divergent to start with [32]. Therefore,  $\Upsilon \rightarrow \chi_{cJ} + X$  as a strictly inclusive decay falls outside the range of applicability of the CS model [54, 55]. Within NRQCD factorization, these CS SDCs are rendered finite by absorbing their IR divergences into the CO LDME  $\langle \mathcal{O}^{\chi_{c0}} ({}^3S_1^{[8]}) \rangle$  associated with the SDC of  $b\bar{b} ({}^3S_1^{[1]}) \rightarrow c\bar{c} ({}^3S_1^{[8]}) + gg$  at LO. Consequently, only the combinations of the  $c\bar{c} ({}^3P_J^{[1]})$  and  $c\bar{c} ({}^3S_1^{[8]})$  channels may be interpreted as physical observables. This mechanism of IR cancellation by NRQCD factorization is familiar, e.g., from hadronic  $h_c$  decay

[56]. Furthermore, Table I tells us that the contributions from  $\chi_{cJ}$  production in association with open charm are greatly suppressed by phase space as expected.

$f_{8,gg}^{\text{LO}}(10^{-4})$	$f_{8,gg}^{\text{corr}}(10^{-4})$	$f_{8,c\bar{c}g}(10^{-5})$
2.38	$4.85 + 13.62 \ln(\frac{\mu}{m_b})$	1.23
$f_{1,ggg}^0(10^{-5})$	$f_{1,ggg}^1(10^{-5})$	$f_{1,ggg}^2(10^{-5})$
-4.18	-2.06	-2.65
$f_{1,c\bar{c}g}^0(10^{-7})$	$f_{1,c\bar{c}g}^1(10^{-7})$	$f_{1,c\bar{c}g}^2(10^{-7})$
1.73	1.04	0.35

TABLE I: Numerical values of  $f_{8,gg/c\bar{c}g}^{\text{LO}}$ ,  $f_{8,gg}^{\text{corr}}$ , and  $f_{1,ggg/c\bar{c}g}^J$ .

In Fig. 6(a), we study the dependencies on the renormalization scale  $\mu$  of  $\hat{\Gamma}_{8,gg}^{\text{LO}}$ ,  $\hat{\Gamma}_{8,gg}^{\text{corr}}$ , and  $\hat{\Gamma}_{8,gg}^{\text{NLO}} = \hat{\Gamma}_{8,gg}^{\text{LO}} + \hat{\Gamma}_{8,gg}^{\text{corr}}$ . As mentioned above,  $\hat{\Gamma}_{8,gg}^{\text{LO}}$  is evaluated with the one-loop expression of  $\alpha_s(\mu)$ , while  $\hat{\Gamma}_{8,gg}^{\text{corr}}$  and  $\hat{\Gamma}_{8,gg}^{\text{NLO}}$  are evaluated with the two-loop expression of  $\alpha_s(\mu)$ . In Fig. 6(b), the factor  $K = \hat{\Gamma}_{8,gg}^{\text{NLO}}/\hat{\Gamma}_{8,gg}^{\text{LO}}$  is shown as a function of  $\mu$ . As expected on general grounds, the  $\mu$  dependence is reduced as we pass from LO to NLO. Unfortunately, the  $\mu$  dependence of  $\hat{\Gamma}_{8,gg}^{\text{NLO}}$  is still appreciable, so that scale optimization appears appropriate. Since the  $\mu$  dependence of  $\hat{\Gamma}_{8,gg}^{\text{NLO}}$  is monotonic, the Principle of Minimal Sensitivity [57] is not applicable. However, the concept of Fastest Apparent Convergence (FAC) [58] works, since the value of  $\mu$  for which  $K = 1$ ,  $\mu_{\text{FAC}}$ , is a typical energy scale of the  $\Upsilon \rightarrow \chi_{cJ} + X$  decays. From Fig. 6, we read off that  $\mu_{\text{FAC}} = 6.2 \text{ GeV}$ . In the following, we will use this as the central scale and estimate the theoretical uncertainty by varying  $\mu$  in the range  $\mu_{\text{FAC}}/2 < \mu < 2\mu_{\text{FAC}}$ .

From Figs. 1–5, we observe that  $\chi_{cJ}$  production from  $\Upsilon$  decay may be viewed, at least at LO, as  $\Upsilon \rightarrow ggg$  decay followed by  $g \rightarrow \chi_{cJ} + X$  via fragmentation. Inspired by this observation, we express the branching ratio  $\mathcal{B}(\Upsilon \rightarrow$



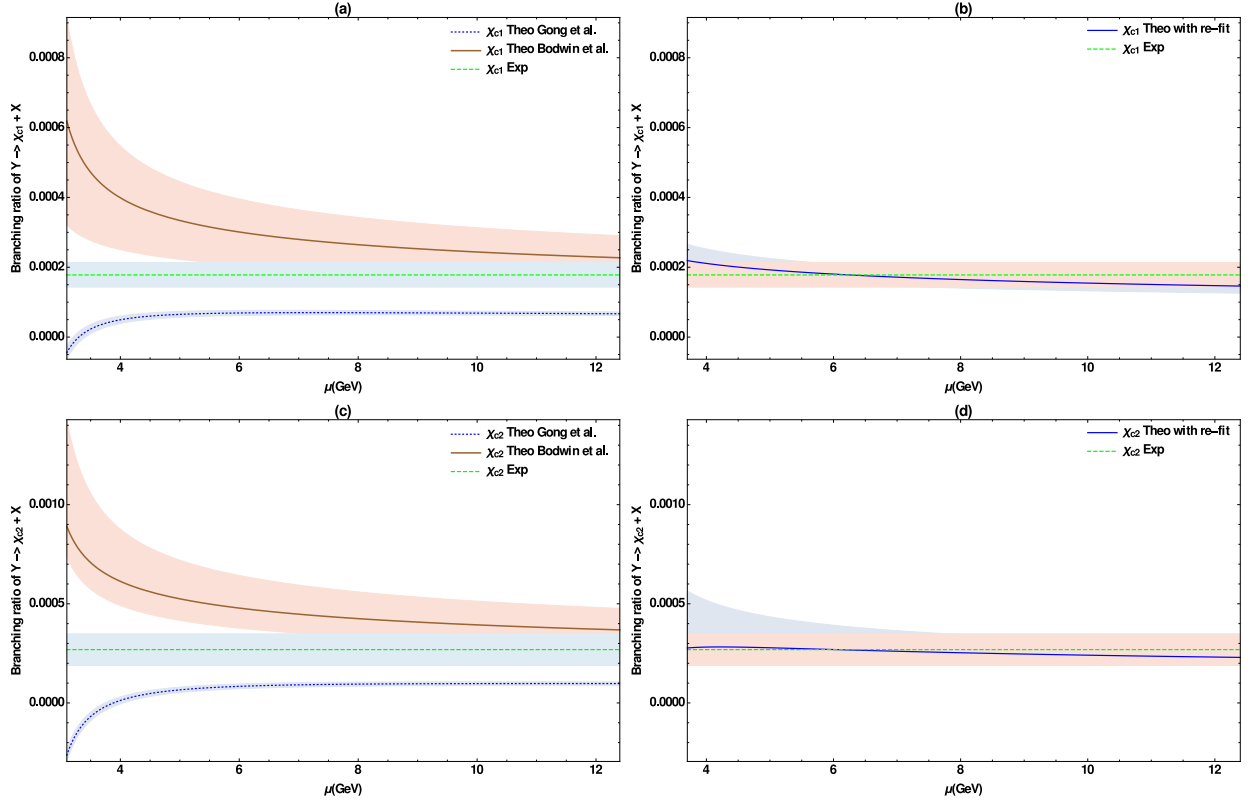


FIG. 7:  $\mu$  dependencies of  $\mathcal{B}(\Upsilon \rightarrow \chi_{c1} + X)$  (upper row) and  $\mathcal{B}(\Upsilon \rightarrow \chi_{c2} + X)$  (lower row) evaluated with different choices of LDMEs, to be compared with experimental values  $\mathcal{B}(\Upsilon \rightarrow \chi_{c1} + X) = (1.78 \pm 0.35) \times 10^{-4}$  and  $\mathcal{B}(\Upsilon \rightarrow \chi_{c2} + X) = (2.69 \pm 0.8) \times 10^{-4}$  [31], respectively.

$\chi_{cJ} + X$ ) as [38, 41]

$$\mathcal{B}(\Upsilon \rightarrow \chi_{cJ} + X) = \frac{\Gamma(\Upsilon \rightarrow \chi_{cJ} + X)}{\Gamma(\Upsilon \rightarrow ggg)} \mathcal{B}(\Upsilon \rightarrow ggg). \quad (28)$$

We evaluate the partial decay width  $\Gamma(\Upsilon \rightarrow ggg)$  through  $\mathcal{O}(\alpha_s^4)$  as [59]

$$\begin{aligned} \Gamma(\Upsilon \rightarrow ggg) &= \frac{20\alpha_s^3(\mu)}{243m_b^2} (\pi^2 - 9) \langle \Upsilon | \mathcal{O}(^3S_1^{[1]}) | \Upsilon \rangle \\ &\times \left\{ 1 + \frac{\alpha_s(\mu)}{\pi} \left[ -19.4 + \frac{3\beta_0}{2} \left( 1.161 + \ln\left(\frac{\mu}{m_b}\right) \right) \right] \right\}, \end{aligned} \quad (29)$$

and use  $\mathcal{B}(\Upsilon \rightarrow ggg) = 81.7\%$  as determined by the Particle Data Group [31]. This has the advantage that the theoretical prediction no longer depends on  $\langle \Upsilon | \mathcal{O}(^3S_1^{[1]}) | \Upsilon \rangle$  and that its dependencies on  $\alpha_s$  and  $m_b$  are significantly suppressed, so that the parametric uncertainty is greatly reduced. By the same token, the  $\mu$  dependence is greatly reduced as well to become quite moderate, as may be seen from Fig. 7 to be discussed below.

In the following, we compare our theoretical predictions thus improved with the experimental results for direct production,  $\mathcal{B}(\Upsilon \rightarrow \chi_{c1} + X) = (1.78 \pm 0.35) \times 10^{-4}$

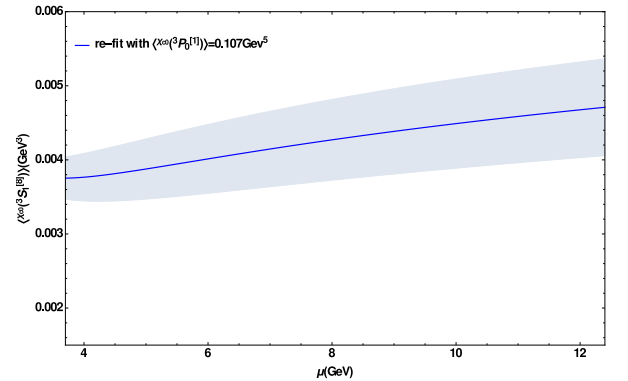


FIG. 8:  $\mu$  dependence of fit value of  $\langle \mathcal{O}^{\chi_{c0}}(^3S_1^{[8]}) \rangle$  for  $\langle \mathcal{O}^{\chi_{c0}}(^3P_0^{[1]}) \rangle = 0.107 \text{ GeV}^5$ .

and  $\mathcal{B}(\Upsilon \rightarrow \chi_{c2} + X) = (2.69 \pm 0.8) \times 10^{-4}$ , obtained from Ref. [31] after subtracting the contributions due to the feed-down from  $\psi(2S)$  mesons. If we adopt the value  $\langle \mathcal{O}^{\chi_{c0}}(^3S_1^{[8]}) \rangle = (2.21 \pm 0.12) \times 10^{-3} \text{ GeV}^3$  from Ref. [17], then our theoretical predictions for  $\mathcal{B}(\Upsilon \rightarrow \chi_{c1} + X)$  and  $\mathcal{B}(\Upsilon \rightarrow \chi_{c2} + X)$ , whose  $\mu$  dependencies are displayed in Figs. 7(a) and (c), respectively, undershoot the experimental data for all values of  $\mu$  in the ballpark of  $\mu_{\text{FAC}}$ .

It is interesting to find out which value of  $\langle \mathcal{O}^{\chi_{c0}}(^3S_1^{[8]}) \rangle$  is favored by the experimental data on  $\mathcal{B}(\Upsilon \rightarrow \chi_{c1} + X)$  and  $\mathcal{B}(\Upsilon \rightarrow \chi_{c2} + X)$ . We, therefore, perform a fit to these data, with the result that

$$\langle \mathcal{O}^{\chi_{c0}}(^3S_1^{[8]}) \rangle = (4.04 \pm 0.47) \times 10^{-3} \text{ GeV}^3, \quad (30)$$

for  $\langle \mathcal{O}^{\chi_{c0}}(^3P_0^{[1]}) \rangle = 0.107 \text{ GeV}^5$  and our default choice  $\mu = \mu_{\text{FAC}}$ . As for the central values, this is about twice as large as the results of Refs. [17, 20]. From Figs. 7(b) and (d), we observe that Eq. (30) yields an excellent description of the measurements of  $\mathcal{B}(\Upsilon \rightarrow \chi_{c1} + X)$  and  $\mathcal{B}(\Upsilon \rightarrow \chi_{c2} + X)$ , respectively, throughout the considered  $\mu$  range,  $3.7 \text{ GeV} < \mu < 2\mu_{\text{FAC}}$ . The lower bound on  $\mu$  is to ensure the positivity of  $\mathcal{B}(\Upsilon \rightarrow \chi_{c0} + X)$ . Thanks to cancellations between the  $^3P_J^{[1]}$  and  $^3S_1^{[8]}$  channels, the  $\mu$  dependencies are relatively mild indicating small theoretical uncertainties.

Vice versa, this feature may be exploited to argue that the theoretical uncertainty in  $\langle \mathcal{O}^{\chi_{c0}}(^3S_1^{[8]}) \rangle$  is small. To this end, we repeat our fit for different values of  $\mu$  and show the outcome in Fig. 8. We read off from Fig. 8 that  $\langle \mathcal{O}^{\chi_{c0}}(^3S_1^{[8]}) \rangle$  ranges from  $(3.7 \pm 0.28) \times 10^{-3} \text{ GeV}^3$  at  $\mu = 3.7 \text{ GeV}$  to  $(4.71 \pm 0.65) \times 10^{-3} \text{ GeV}^3$  at  $\mu = 2\mu_{\text{FAC}}$ . Obviously, the theoretical uncertainty is comparable to the experimental one.

In Ref. [60], an alternative set of  $\chi_{cJ}$  production LDMEs was obtained by fitting cross sections of prompt  $\chi_{c1}$  and  $\chi_{c2}$  hadroproduction measured by ATLAS [61] using NLO SDCs in combination with leading-power fragmentation functions:

$$\begin{aligned} \frac{\langle \mathcal{O}^{\chi_{c0}}(^3P_0^{[1]}) \rangle}{m_c^2} &= (3.53 \pm 1.08) \times 10^{-2} \text{ GeV}^3, \\ \langle \mathcal{O}^{\chi_{c0}}(^3S_1^{[8]}) \rangle &= (5.74 \pm 1.31) \times 10^{-3} \text{ GeV}^3. \end{aligned} \quad (31)$$

The resulting predictions for  $\mathcal{B}(\Upsilon \rightarrow \chi_{c1} + X)$  and  $\mathcal{B}(\Upsilon \rightarrow \chi_{c2} + X)$ , which are also included in Figs. 7(a) and (c), respectively, overshoot the experimental data for  $\mu < \mu_{\text{FAC}}$ , but the error bands overlap for  $\mu \gtrsim \mu_{\text{FAC}}$ .

#### Appendix A: Master Integrals at $\mathcal{O}(\epsilon)$

In the following, we will drop all imaginary parts, since only the real parts contribute to the NLO corrections. We adopt the notation of Ref. [62],

$$\begin{aligned} I_1^D(m_1^2) &= \frac{\mu^{4-D}}{i\pi^{\frac{D}{2}} r_\Gamma} \int d^D l \frac{1}{l^2 - m_1^2 + i\varepsilon}, \\ I_2^D(p_1^2; m_1^2, m_2^2) &= \frac{\mu^{4-D}}{i\pi^{\frac{D}{2}} r_\Gamma} \int d^D l \frac{1}{(l^2 - m_1^2 + i\varepsilon) [(l + p_1)^2 - m_2^2 + i\varepsilon]}, \end{aligned} \quad (A1)$$

where  $r_\Gamma = \Gamma^2(1 - \epsilon)\Gamma(1 + \epsilon)/\Gamma(1 - 2\epsilon) = 1 - \epsilon\gamma_E + \epsilon^2(\gamma_E^2/2 - \pi^2/12) + \mathcal{O}(\epsilon^3)$ . The tadpole integral is given by

$$I_1^D(m^2) = m^2 \left( \frac{\mu^2}{m^2} \right)^\epsilon \left[ \frac{1}{\epsilon} + 1 + \epsilon \left( 1 + \frac{\pi^2}{6} \right) \right]. \quad (A2)$$

#### IV. SUMMARY

In this work, we studied the inclusive decays  $\Upsilon \rightarrow \chi_{cJ} + X$  through  $\mathcal{O}(\alpha_s^5)$  and to LO in  $v_c$  and  $v_b$  in the NRQCD [1] factorization approach [2]. According to the velocity scaling rules [3], we thus included the Fock states  $b\bar{b}(^3S_1^{[1]})$ ,  $c\bar{c}(^3P_J^{[1]})$ , and  $c\bar{c}(^3S_1^{[8]})$ . Besides gluons and light quarks, we also allowed for open charm to appear in the hadronic debris  $X$ . Since the partonic subprocess  $b\bar{b}(^3S_1^{[1]}) \rightarrow c\bar{c}(^3S_1^{[8]}) + gg$  already contributes at  $\mathcal{O}(\alpha_s^4)$ , we calculated its quantum corrections at NLO. Since the dependencies of the branching ratios  $\mathcal{B}(\Upsilon \rightarrow \chi_{cJ} + X)$  on the renormalization scale  $\mu$  turned out to be monotonic, we applied scale optimization via FAC [58], which led to  $\mu_{\text{FAC}} = 6.2 \text{ GeV}$ . We then estimated the theoretical uncertainty by varying  $\mu$  in the range between  $\mu_{\text{FAC}}/2$  and  $2\mu_{\text{FAC}}$ . Using as input the value  $\langle \mathcal{O}^{\chi_{c0}}(^3P_0^{[1]}) \rangle = 0.107 \text{ GeV}^5$  obtained in Ref. [52] for the Buchmüller-Tye potential [53], we fitted  $\langle \mathcal{O}^{\chi_{c0}}(^3S_1^{[8]}) \rangle$  to experimental data of  $\mathcal{B}(\Upsilon \rightarrow \chi_{c1} + X)$  and  $\mathcal{B}(\Upsilon \rightarrow \chi_{c2} + X)$  via direct production [31] to find the value quoted in Eq. (30). This exceeds the fit results of Refs. [17, 20] by roughly a factor of two but is compatible with the lower bound extracted in Ref. [60]. Further experimental and theoretical efforts are required to solve this discrepancy.

#### Acknowledgments

We would like to thank M. Butenschön for useful discussions. This work was supported in part by the German Federal Ministry for Education and Research BMBF through Grant No. 05H15GUCC1 and by the China Scholarship Council CSC through Grant No. CSC-201404910576.



The bubble integral with two vanishing masses is given by

$$I_2^D(s; 0, 0) = \left(\frac{\mu^2}{s}\right)^\epsilon \left[ \frac{1}{\epsilon} + 2 + \epsilon \left( 4 - \frac{\pi^2}{2} \right) \right]. \quad (\text{A3})$$

The bubble integral with one vanishing mass is given by

$$I_2^D(s; 0, m^2) = \left(\frac{\mu^2}{m^2}\right)^\epsilon \left[ \frac{1}{\epsilon} - d_1 + \epsilon \left( \frac{d_2}{2} + \frac{\pi^2}{6} \right) \right], \quad (\text{A4})$$

where

$$d_1 = \frac{s - m^2}{s} \ln \frac{|m^2 - s|}{m^2} - 2, \quad (\text{A5})$$

and

$$d_2 = 2 \frac{s - m^2}{s} \left( \ln \frac{m^2 - s}{m^2} \ln \frac{m^2 - s}{|s|} - 2 \ln \frac{m^2 - s}{m^2} - \text{Li}_2 \left( \frac{m^2 - s}{m^2} \right) + \frac{\pi^2}{6} \right) + 8 \quad (\text{A6})$$

for  $s < m^2$  and

$$d_2 = \frac{s - m^2}{s} \left( \ln^2 \frac{s - m^2}{m^2} + \ln^2 \frac{s - m^2}{s} - 4 \ln \frac{s - m^2}{m^2} + 2 \text{Li}_2 \left( \frac{s - m^2}{s} \right) - \frac{5\pi^2}{3} \right) + 8 \quad (\text{A7})$$

for  $s > m^2$ . The bubble integral with two different masses is given by

$$I_2^D\left(\frac{t}{4}; m_c^2, m_b^2\right) = \left(\frac{\mu^2}{t/4}\right)^\epsilon \left[ \frac{1}{\epsilon} - c_1 + \epsilon \left( \frac{c_2}{2} + \frac{\pi^2}{6} \right) \right], \quad (\text{A8})$$

where

$$\begin{aligned} c_1 &= -\frac{1}{t} \left[ -a \ln \frac{s + u - a}{8m_c m_b} + 2(m_b^2 - m_c^2) \ln \frac{m_c^2}{m_b^2} + t \ln \frac{t}{4m_c m_b} \right] - 2, \\ c_2 &= \frac{2a}{t} \left[ \ln \frac{s + u + a}{8m_c^2} \left( \ln \frac{a - s_b - u_b}{2a} + \ln \frac{t}{4m_b^2} + 2 \right) + \frac{1}{2} \ln^2 \frac{s + u + a}{8m_c^2} + \text{Li}_2 \left( \frac{s_b + u_b + a}{2a} \right) \right. \\ &\quad \left. - \text{Li}_2 \left( \frac{-s_c - u_c + a}{2a} \right) \right] + \frac{s_c + u_c + a}{t} \ln \frac{m_c^2}{m_b^2} \left( \ln \frac{t}{4m_c m_b} + 2 \right) + \left( \ln \frac{t}{4m_b^2} + 2 \right)^2 + 4. \end{aligned} \quad (\text{A9})$$

## Appendix B: Soft Integrals

To extract the IR divergences of the real corrections in the limit  $k_5 \rightarrow 0$ , we need to know the results of the following integrals:

$$\begin{aligned} \int_{\text{soft}} \frac{d\text{PS}_{k_5}}{(K \cdot k_5)^2} &= \frac{C_\epsilon}{32\pi^2 m_c^2} \left( -\frac{1}{\epsilon} - \frac{s_c + u_c}{a} \ln \frac{s_c + u_c + a}{s_c + u_c - a} - \ln \frac{\mu^2}{4\delta_s^2 m_c^2} \right), \\ \int_{\text{soft}} \frac{d\text{PS}_{k_5}}{(k_3 \cdot k_5)(k_4 \cdot k_5)} &= \frac{C_\epsilon}{4\pi^2 t} \left( \frac{1}{\epsilon^2} + \frac{1}{\epsilon} \ln \frac{\mu^2}{4\delta_s^2 m_c^2} + \frac{1}{2} \ln^2 \frac{\mu^2}{4\delta_s^2 m_c^2} - \frac{\pi^2}{4} \right), \\ \int_{\text{soft}} \frac{d\text{PS}_{k_5}}{(K \cdot k_5)(k_3 \cdot k_5)} &= \frac{C_\epsilon}{8\pi^2 s_c} \left[ \frac{1}{\epsilon^2} + \frac{1}{\epsilon} \ln \frac{\mu^2 t}{s_c^2 \delta_s^2} + \ln^2 \frac{s_c + u_c - a}{2s_c} + \frac{1}{2} \ln^2 \frac{\mu^2}{4\delta_s^2 m_c^2} - \ln \frac{s_c^2}{4m_c^2 t} \ln \frac{\mu^2}{4\delta_s^2 m_c^2} \right. \\ &\quad \left. - \frac{1}{2} \ln^2 \frac{s_c + u_c + a}{s_c + u_c - a} + 2 \text{Li}_2 \left( -\frac{s - u + a}{s_c + u_c - a} \right) - 2 \text{Li}_2 \left( \frac{s - u - a}{2s_1} \right) - \frac{\pi^2}{4} \right], \\ \int_{\text{soft}} \frac{d\text{PS}_{k_5}}{(K \cdot k_5)(k_4 \cdot k_5)} &= \frac{C_\epsilon}{8\pi^2 u_c} \left[ \frac{1}{\epsilon^2} + \frac{1}{\epsilon} \ln \frac{\mu^2 t}{u_c^2 \delta_s^2} + \ln^2 \frac{s_c + u_c - a}{2u_c} + \frac{1}{2} \ln^2 \frac{\mu^2}{4\delta_s^2 m_c^2} - \ln \frac{u_c^2}{4m_c^2 t} \ln \frac{\mu^2}{4\delta_s^2 m_c^2} \right. \\ &\quad \left. - \frac{1}{2} \ln^2 \frac{s_c + u_c + a}{s_c + u_c - a} + 2 \text{Li}_2 \left( -\frac{u - s + a}{s_c + u_c - a} \right) - 2 \text{Li}_2 \left( \frac{u - s - a}{2u_c} \right) - \frac{\pi^2}{4} \right]. \end{aligned} \quad (\text{B1})$$

---

[1] W. E. Caswell and G. P. Lepage, Phys. Lett. **167B**, 437 (1986).

[2] G. T. Bodwin, E. Braaten, and G. P. Lepage, Phys. Rev.

- D **51**, 1125 (1995); **55**, 5853(E) (1997).
- [3] G. P. Lepage, L. Magnea, C. Nakhleh, U. Magnea, and K. Hornbostel, Phys. Rev. D **46**, 4052 (1992).
  - [4] N. Brambilla *et al.*, Eur. Phys. J. C **71**, 1534 (2011).
  - [5] N. Brambilla *et al.*, Eur. Phys. J. C **74**, 2981 (2014).
  - [6] Y.-J. Zhang, Y.-Q. Ma, K. Wang, and K.-T. Chao, Phys. Rev. D **81**, 034015 (2010).
  - [7] Y.-Q. Ma, Y.-J. Zhang, and K.-T. Chao, Phys. Rev. Lett. **102**, 162002 (2009).
  - [8] B. Gong and J.-X. Wang, Phys. Rev. Lett. **102**, 162003 (2009).
  - [9] M. Klasen, B. A. Kniehl, L. N. Mihaila, and M. Steinhauser, Nucl. Phys. **B713**, 487 (2005); Phys. Rev. D **71**, 014016 (2005).
  - [10] M. Butenschoen and B. A. Kniehl, Phys. Rev. D **84**, 051501(R) (2011).
  - [11] M. Butenschön and B. A. Kniehl, Phys. Rev. Lett. **104**, 072001 (2010).
  - [12] M. Butenschoen and B. A. Kniehl, Phys. Rev. Lett. **107**, 232001 (2011).
  - [13] Y.-Q. Ma, K. Wang, and K.-T. Chao, Phys. Rev. Lett. **106**, 042002 (2011).
  - [14] M. Butenschön and B. A. Kniehl, Phys. Rev. Lett. **106**, 022003 (2011).
  - [15] M. Butenschoen and B. A. Kniehl, Phys. Rev. Lett. **108**, 172002 (2012).
  - [16] K.-T. Chao, Y.-Q. Ma, H.-S. Shao, K. Wang, and Y.-J. Zhang, Phys. Rev. Lett. **108**, 242004 (2012).
  - [17] B. Gong, L.-P. Wan, J.-X. Wang, and H.-F. Zhang, Phys. Rev. Lett. **110**, 042002 (2013).
  - [18] H.-S. Shao, H. Han, Y.-Q. Ma, C. Meng, Y.-J. Zhang, and K.-T. Chao, J. High Energy Phys. 05 (2015) 103.
  - [19] M. Butenschoen, Z.-G. He, and B. A. Kniehl, Phys. Rev. Lett. **114**, 092004 (2015).
  - [20] Y.-Q. Ma, K. Wang, and K.-T. Chao, Phys. Rev. D **83**, 111503(R) (2011).
  - [21] D. Li, Y.-Q. Ma, and K.-T. Chao, Phys. Rev. D **83**, 114037 (2011).
  - [22] H.-S. Shao, Y.-Q. Ma, K. Wang, and K.-T. Chao, Phys. Rev. Lett. **112**, 182003 (2014).
  - [23] H.-F. Zhang, L. Yu, S.-X. Zhang, and L. Jia, Phys. Rev. D **93**, 054033 (2016); **93**, 079901(E) (2016).
  - [24] L.-B. Chen, J. Jiang, and C.-F. Qiao, Phys. Rev. D **91**, 094031 (2015).
  - [25] C. Zhou, G. Li, M. Song, W.-G. Ma, and R.-Y. Zhang, Phys. Rev. D **94**, 094045 (2016).
  - [26] M. Beneke, F. Maltoni, and I. Z. Rothstein, Phys. Rev. D **59**, 054003 (1999).
  - [27] Z.-G. He and B.-Q. Li, Phys. Lett. B **693**, 36 (2010).
  - [28] B.-Q. Li, R. Li, and Z.-G. He, Chin. Phys. C **34**, 521 (2010).
  - [29] S. Jia *et al.* (Belle Collaboration), Phys. Rev. D **95**, 012001 (2017).
  - [30] R. A. Briere *et al.* (CLEO Collaboration), Phys. Rev. D **70**, 072001 (2004).
  - [31] C. Patrignani *et al.* (Particle Data Group), Chin. Phys. C **40**, 100001 (2016).
  - [32] H. D. Trottier, Phys. Lett. B **320**, 145 (1994).
  - [33] K. Cheung, W.-Y. Keung, and T. C. Yuan, Phys. Rev. D **54**, 929 (1996).
  - [34] K. Abe *et al.* (Belle Collaboration), Phys. Rev. Lett. **89**, 142001 (2002).
  - [35] K.-Y. Liu, Z.-G. He, and K.-T. Chao, Phys. Rev. D **69**, 094027 (2004).
  - [36] Y.-J. Zhang and K.-T. Chao, Phys. Rev. Lett. **98**, 092003 (2007).
  - [37] B. Gong and J.-X. Wang, Phys. Rev. D **80**, 054015 (2009).
  - [38] Z.-G. He and J.-X. Wang, Phys. Rev. D **81**, 054030 (2010).
  - [39] Z.-G. He, B. A. Kniehl, and X.-P. Wang, to be published.
  - [40] M. Napsuciale, Phys. Rev. D **57**, 5711 (1998).
  - [41] Z.-G. He and J.-X. Wang, Phys. Rev. D **82**, 094033 (2010).
  - [42] T. Hahn, Comput. Phys. Commun. **140**, 418 (2001).
  - [43] R. Mertig, M. Böhm, and A. Denner, Comput. Phys. Commun. **64**, 345 (1991).
  - [44] J. Kuipers, T. Ueda, J. A. M. Vermaseren, and J. Vollinga, Comput. Phys. Commun. **184**, 1453 (2013).
  - [45] F. Feng, MATHEMATICA Apart Comput. Phys. Commun. **183**, 2158 (2012).
  - [46] A. V. Smirnov, J. High Energy Phys. 10 (2008) 107.
  - [47] S. Carrazza, R. K. Ellis, and G. Zanderighi, Comput. Phys. Commun. **209**, 134 (2016).
  - [48] T. Hahn, Comput. Phys. Commun. **168**, 78 (2005).
  - [49] B. W. Harris and J. F. Owens, Phys. Rev. D **65**, 094032 (2002).
  - [50] R. Kumar, Phys. Rev. **185**, 1865 (1969).
  - [51] M. Butenschön, University of Hamburg Report No. DESY-THESIS-2009-021.
  - [52] E. J. Eichten and C. Quigg, Phys. Rev. D **52**, 1726 (1995).
  - [53] W. Buchmüller and S.-H. H. Tye, Phys. Rev. D **24**, 132 (1981).
  - [54] E. L. Berger and D. Jones, Phys. Rev. D **23**, 1521 (1981).
  - [55] R. Baier and R. Rückl, Phys. Lett. **102B**, 364 (1981).
  - [56] H.-W. Huang and K.-T. Chao, Phys. Rev. D **54**, 3065 (1996); **56**, 7472(E) (1997); **60**, 079901(E) (1999).
  - [57] P. M. Stevenson, Phys. Lett. **100B**, 61 (1981); Phys. Rev. D **23**, 2916 (1981); Nucl. Phys. **B203**, 472 (1982).
  - [58] G. Grunberg, Phys. Lett. **95B**, 70 (1980); **110B**, 501(E) (1982).
  - [59] P. B. Mackenzie and G. P. Lepage, Phys. Rev. Lett. **47**, 1244 (1981).
  - [60] G. T. Bodwin, K.-T. Chao, H. S. Chung, U.-R. Kim, J. Lee, and Y.-Q. Ma, Phys. Rev. D **93**, 034041 (2016).
  - [61] G. Aad *et al.* (ATLAS Collaboration), J. High Energy Phys. 07 (2014) 154.
  - [62] R. K. Ellis and G. Zanderighi, J. High Energy Phys. 02 (2008) 002.